Quantum Electronics **52** (3) 233–246 (2022)

https://doi.org/10.1070/QEL18000

Light bullets in transparent dielectrics

V.P. Kandidov, E.D. Zaloznaya, A.E. Dormidonov, V.O. Kompanets, S.V. Chekalin

Abstract. **This paper presents a retrospective analysis of the development of notions in nonlinear optics: from beam self-focusing and pulse filamentation to light bullets – wave packets extremely compressed in space and time during laser light propagation in the bulk of a transparent medium. We describe the state of the art in studies of mid-IR light bullets in condensed media and air.**

Keywords: *self-focusing, filamentation, light bullets, supercontinuum, anti-Stokes wing, wave packet.*

1. Introduction

The light bullet (LB) phenomenon lies in the area of nonlinear optics of femtosecond pulses. LBs result from coupled processes of wave packet self-focusing in space and self-compression in time, which occur at an anomalous group velocity dispersion in the bulk of a third-order nonlinear medium under laser plasma generation conditions. A light bullet is characterised by strong spatiotemporal optical field localisation: the space and temporal scales of the localisation region are a few wavelengths and one or two optical oscillation periods. Unlike in planar waveguides, optical fibre, photonic crystals, and other guiding structures, which ensure dispersion for spatial modes [1], group velocity dispersion in the bulk of a medium is determined by the optical properties of the transparent dielectric. At present, the possibility of obtaining light bullets with strong localisation of optical radiation is of considerable interest for developing methods of diagnosing processes with high spatial and temporal resolution.

2. Beam self-focusing

Self-focusing of light beams, which plays a key role in LB formation, was predicted by Askar'yan in 1961 [2] and granted a patent for an invention with the following formula: "...electromagnetic and acoustic beam self-focusing phenomenon consisting in a decrease in beam divergence (or an increase in beam convergence) due to a transverse nonlinear refractive index gradient and the formation of a nonlinear waveguide, which reduces the cross section of the beam". Beam self-focusing seemed to open up great possibilities for optical radiation channelling and transmission over long distances without losses and attracted much attention. Beam self-focusing was first detected by Pilipetskii and Rustamov [3] in experiments carried out at Moscow State University and dealing with the propagation of nanosecond 1.06-μm pulses of 20 MW power in cyclohexane-filled cuvettes. At the same time, it is worth noting that foreign sources associate the first observation of self-focusing with Hercher's report dealing with damage to glass by focused light, which was previously only mentioned in a conference program [4]. In this report, which was first published as late as 2009 [5], self-focusing is not discussed at all. Laser beam self-focusing in air was first detected at the Lebedev Physical Institute, USSR Academy of Sciences, by Basov et al. [6], who studied free-space propagation of picosecond 1.06-μm pulses of 10^{12} W power over 25 m.

A defining contribution to theoretical studies of self-focusing was made by the pioneering work by Townes (see e.g. Ref. [7]) and Talanov [8], who estimated the critical light beam self-focusing power and examined modulation instability of light waves in a nonlinear Kerr medium, and work by Zakharov et al. [9], who formulated a condition for light beam channelling in a nonlinear medium. An effective tool for analytical studies of self-focusing is the paraxial approximation of the aberration-free method of nonlinear quasi-optics, developed by Akhmanov, Sukhorukov, and Khokhlov [10, 11]. Analytical estimates of the critical power for self-focusing and the self-focusing distance gave way to phenomenological formulas obtained by approximating results obtained by numerically solving a quasi-optics equation for a beam in a Kerr medium [8, 12]. At present, the critical power for self-focusing of a collimated Gaussian beam, P_{cr}, in a third-order inertialess medium is given by

$$P_{cr} = 3.77\frac{\pi n_0}{2k^2 n_2}, \tag{1}$$

where n_0 is the refractive index; n_2 is the nonlinearity coefficient; and k is the wavenumber. It is worth noting that the lowest critical power for self-focusing corresponds to the Townes mode, which is a steady-state solution to the parabolic equation for a beam in a third-order nonlinear medium [7]. Moreover, the profile of a Gaussian beam is similar to the Townes mode, and its critical power P_{cr} differs from the minimum value by less than 1.5%. As the distinction of the beam profile from a Gaussian shape increases, so does P_{cr} [13]. The

V.P. Kandidov, E.D. Zaloznaya Faculty of Physics, Lomonosov Moscow State University, Leninskie gory 1, 119991 Moscow, Russia; Institute of Spectroscopy, Russian Academy of Sciences, Fizicheskaya ul. 5, Troitsk, 108840 Moscow, Russia;
e-mail: kandidov@physics.msu.ru, ed.zaloznaya@physics.msu.ru;
A.E. Dormidonov, V.O. Kompanets, S.V. Chekalin Institute of Spectroscopy, Russian Academy of Sciences, Fizicheskaya ul. 5, Troitsk, 108840 Moscow, Russia

Received 11 December 2021
Kvantovaya Elektronika **52** (3) 233–246 (2022)
Translated by O.M. Tsarev

steady-state self-focusing distance of a collimated Gaussian beam of radius a_0 is given by a relation first derived by Gol'dberg et al. [14], which was later slightly modified and named the Marburger formula [12]:

$$L_{\rm nl} = \frac{0.367ka_0^2}{\{[(P_{\rm peak}/P_{\rm cr})^{1/2} - 0.852]^2 - 0.0219\}^{1/2}}, \qquad (2)$$

where $P_{\rm peak}$ is the peak beam power. Relation (2) for the self-focusing distance can be generalised to include elliptical Gaussian beams by substituting the critical power $P_{\rm cr}(a, b)$ for an elliptical profile with semiaxes a and b [15].

The moving-focus model, proposed by Prokhorov and his colleagues (see e.g. Refs [16, 17]), provided clear physical interpretation of thin filaments resulting from transient nanosecond pulse self-focusing. According to this model, temporal pulse slices, starting from the peak power slice, are independently focused in the medium to form a thread of foci in the propagating pulse. In this process, two-photon absorption in the foci limits the collapsing increase in intensity and rules out any effect of the temporal pulse slices on each other. In the case of transient self-focusing, an appreciable contribution to the transformation of the pulse is made by an envelope shock wave, which appears on the trailing edge of a short pulse upon a nonlinear group velocity decrease in a Kerr medium [18, 19]. At present, this effect, referred to as pulse self-steepening, is an integral part of generally accepted theoretical models for self-focusing and filamentation of femtosecond pulses.

By the 1960s–1970s, it became clear that self-focusing failed to ensure lossless transport of localised laser beam energy over large distances. Moreover, beam self-focusing in solid-state amplifiers was accompanied by an increase in nonlinear loss, which limited the power of systems under development. Small-scale self-focusing caused by modulation instability [20] resulted in the formation of a divergent 'halo' in the beam, which consumed a large part of the energy of the pulse being amplified, and specialised spatial filtering and disc amplifier schemes were designed to suppress it [21]. At the same time, in the case of short pulse generation the self-focusing effect in active media leads to passive mode locking, which underlies the operation of femtosecond pulse generators in state-of-the-art lasers [22].

3. Pulse filamentation

3.1. Retrospective

The significant advances in femtosecond laser engineering in the second half of the 1990s renewed interest in the self-focusing phenomenon. The use of femtosecond gigawatt Ti:sapphire laser pulses allowed extended highly localised light filaments resulting from transient self-focusing to be studied in air. The peak power of femtosecond near-IR pulses with an energy of several tens of millijoules reaches tens of gigawatts and more, which is above the critical power for self-focusing in air. Note that the characteristic response time of low-threshold nonlinear effects associated with adiabatic and isothermal processes of absorbed laser energy thermalisation and breakdown development considerably exceeds the pulse duration, so these effects have no influence on femtosecond beam self-focusing [23]. In the case of femtosecond pulses, nonlinear interaction in transparent dielectrics is determined by the electronic response with a characteristic time $\tau \sim 1$ fs, which can be thought of as instantaneous; by stimulated Raman scattering by rotational transitions of molecules of the medium, which is an inertial process; and by refraction in the laser-induced plasma, whose generation as a result of photoionisation and avalanche ionisation in condensed media takes of the order of 1 fs. The characteristic setting time of the Raman response in air, $\tau \approx 70$ fs, was first calculated by Oleinikov and Platonenko [24]. Unfortunately, their report was subsequently forgotten: by Nibberring et al. [25], who reproduced their results and evaluated the relative contribution that the Raman response makes to third-order nonlinearity; by Mlejnek et al. [26], who derived an approximate formula for mathematical models of filamentation; and by Zheltikov [27], who examined the effect of vibrational levels on the Raman response.

In the first experiments dealing with femtosecond filamentation in air in the 1990s [28–30], the laser beam radius was found to decrease, which took place over a distance of several tens of metres; divergent broadband conical emission and nonmonotonic variation in energy density along the filament, due to refocusing, were observed; and the first estimates of the electron density in the laser-induced plasma were made. To date, femtosecond light filamentation has been studied in detail both experimentally and theoretically. The results of fundamental studies of the filamentation phenomenon and analysis of its practical applications were summarised in a number of reviews [31–35].

Luminescence of the plasma generated by light in a filament allows its track to be visualised via multipulse exposure. Images of a femtosecond filament in gases and condensed media are similar to the nanosecond light self-focusing picture observed in the first experiment (Fig. 1).

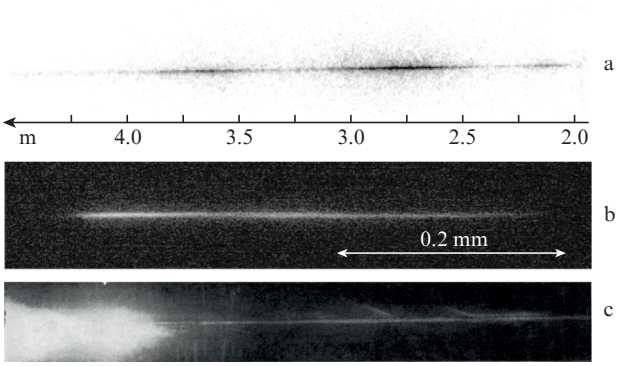

Figure 1. Images of a filament in the case of (a) a pulse (0.8 μm, 45 fs, 13 mJ) propagating in air (from right to left) and focused by an $F = 5$ m lens [31], (b) a pulse (0.8 μm, 130 fs, 1–2 μJ) propagating in fused silica (from left to right) ($F = 0.1$ m) [36], and a pulse (1.06 μm, 20 MW) propagating in cyclohexane (from left to right) ($F = 0.028$ m) [3].

3.2. Investigation techniques

In experimental studies of femtosecond filamentation, along with the simplest measurements of the surface optical energy flux density (fluence) distribution in the plane of a transverse section, electromagnetic, optical, and nonlinear-optical methods have been developed. To measure the electron density in a laser-induced plasma, use is made of electromagnetic methods (capacitance [37, 38], conductive channel [39–42], and electromagnetic induction [43] methods) and optical methods

(interference [44, 45] and diffractometric [41] methods and shadowgraphy with high spatial and temporal resolution [46–48]). For time-resolved measurements of the 3D filament intensity distribution, nonlinear optical methods are used: femtosecond polarography [49–51] and nonlinear mixing [52–54]. Acoustic measurements [55, 56] are used to study filament light absorption in air, and optoacoustic tomography [57] is used for remote determination of filament position in space. Laser colouration opens up fundamentally new possibilities for experimental studies of filamentation. This method allows one to record the spatial filament intensity distribution via single-pulse exposure, which rules out uncertainties related to probe beam fluctuations [58, 59]. The use of wedge-shaped samples translated across the light propagation direction in the experimental configuration allows one to investigate filamentation development over distance, like in free-space experiments [60–62].

In numerical studies of femtosecond filamentation, the slowly varying amplitude method with second-order dispersion theory gave way in the 2000s to the slowly varying wave approximation, in which the next terms in the expansion in terms of time derivatives of the complex field amplitude are retained. This allows one to examine pulses whose duration is comparable to the optical oscillation period [63]. This approximation was used to construct a numerical model which, in the case of light filamentation, describes the increase in the slope of the trailing edge, the formation of a shock wave of the pulse envelope, nonlinear response retardation in the case of Raman scattering, laser plasma generation as a result of photoionisation and avalanche processes, and, finally, dispersion in the Sellmeier approximation [64, 65]. At present, a numerical method based on a unidirectional Maxwell equation is being increasingly widely used [32, 33, 66]. In this method, an equation for the spectrum of the electric field intensity describes all wave effects of light propagation, with no limitations on pulse duration, which makes it possible, in conjunction with the constitutive equation describing nonlinear optical interaction, to construct an adequate model for filamentation and light bullet formation during propagation of femtosecond pulses in condensed media and gases.

3.3. Filamentation scenario

In the case of femtosecond filamentation, the collapsing growth of intensity due to Kerr self-focusing is limited by defocusing in the laser-induced plasma. As a result, the saturation intensity in the filament is 10^{13} to 10^{14} W cm^{-2} in gases and condensed media. Note that plasma generation via photoionisation by IR radiation is a multiphoton process and has a threshold character because the ionisation potential of gases or the band gap of many dielectrics considerably exceeds the photon energy. A femtosecond filament results from a dynamic balance between the Kerr self-focusing of light and its aberration defocusing in the laser plasma, whose density rises sharply as the intensity reaches the ionisation threshold. The electron density is then relatively low: $(10^{-3} - 10^{-5})N_0$, where N_0 is the density of neutrals. The multiphoton generation process leads to plasma formation in the axial region of the filament with a high light intensity, and the plasma channel diameter is approximately a factor of $\sqrt{K}$ smaller (where K is the multiphoton ionisation order) than the transverse size of the optical field localisation region (Fig. 2). At this relationship between the geometric parameters in the filament,

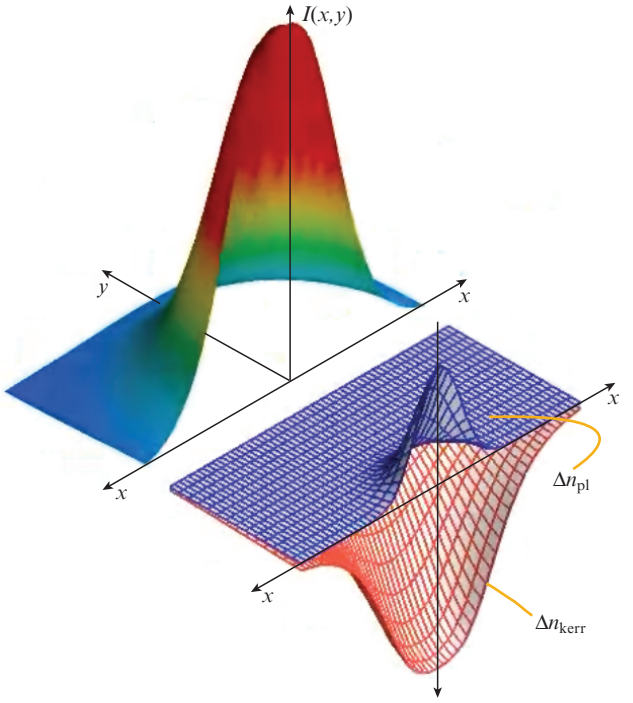

Figure 2. (Colour online) Distributions of intensity $I(x, y)$ and the refractive index changes due to Kerr $[\Delta n_{\text{Kerr}}(x, y)]$ and plasma $[\Delta n_{\text{pl}}(x, y)]$ nonlinearities in the plane of a transverse section in the case of intensity saturation in a filament forming in air during propagation of a 100-fs pulse at a wavelength of 0.8 μm with a radius of 1.2 mm and peak power of 14.5 GW [67].

the optical powers of the nonlinear Kerr and plasma lenses are equal in magnitude [68]. The filament diameter, as evaluated from the localisation region of a strong optical field, is about 100 μm in air and 10 μm in condensed media, and the plasma channel diameter can be estimated at 20–80 and 5–10 μm, respectively.

In the case of collimated light, the filament length reaches tens of metres in air and several millimetres in condensed media, which considerably exceeds the Rayleigh length for beams having the same diameter as the filament. Light localisation in an extended filament is maintained by the optical field that spans the localisation region and is referred to as an energy reservoir. The crucial role of the energy reservoir in the formation of an extended filament was demonstrated by experiments carried out by Dubietis et al. [69] with a pinhole and shield, which isolated and blocked, respectively, the light localisation region in the filament (Fig. 3). After the energy reservoir is blocked in the peripheral part of the beam, the filament behind the pinhole disappears (Fig. 3a), whereas after blocking the axial region it appears again (Fig. 3b), and the energy density distribution turns out to be similar to that in the case of free-filament propagation (Fig. 3c).

The physical scenario of light localisation upon pulse self-focusing and the role of the energy reservoir in the formation of an extended filament are illustrated by the moving-focus model [16, 17]. According to this model, temporal pulse slices, starting from the peak power slice, are sequentially focused to form a filament. In this process, the temporal slices of the leading edge, whose power decreases with displacement from the centre of the pulse, are focused at a larger distance (Fig. 4). The light at the periphery of these temporal slices is a reser-

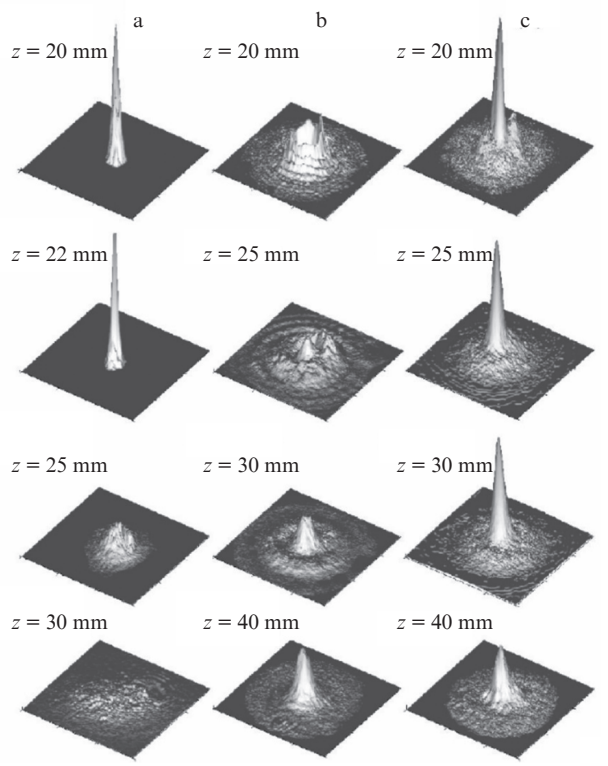

Figure 3. Surface energy density (fluence) distributions at various distances z for filamentation of a 200-fs pulse with a wavelength of 0.527 μm and energy of 3 μJ in water: (a) after a 55-μm-diameter pinhole, (b) after a 55-μm-diameter shield, (c) free-filament propagation [69].

voir of energy localised in the extended filament. Note that, unlike in the classic moving-focus model, the transformation of the temporal slices during pulse filamentation is not independent. The increase in intensity in the focused temporal slices on the leading edge causes generation of a plasma, which leads to defocusing of subsequent slices (Fig. 5). Aberration defocusing of light in the laser-induced plasma entails the formation of a ring structure in the trailing part of the pulse. During pulse propagation, it may contract to the axis as a consequence of Kerr refocusing. As a result, the power in a transverse section of a temporal pulse slice contracts to the axis upon self-focusing, then flows to the axial region upon defocusing in the plasma, and localises again on the axis upon refocusing (Fig. 6) [70]. As a result of the refocusing, the fluence on the filament axis varies nonmonotonically with distance [30].

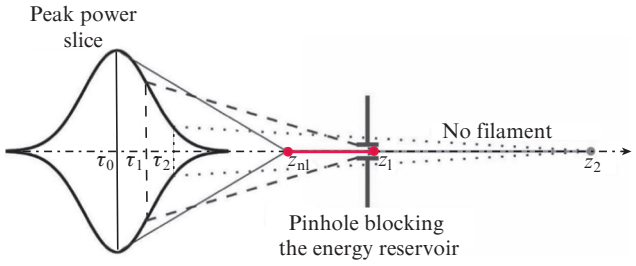

Figure 4. (Colour online) Moving-focus model clarifying the role of the energy reservoir in the formation of an extended filament during pulse propagation.

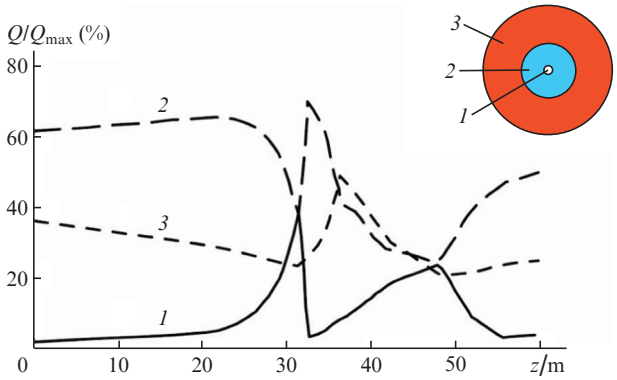

Figure 5. (Colour online) Variation of the relative power Q/Q_{max} with distance in various regions of a transverse section of a temporal pulse slice: Kerr focusing at a distance z = 30 m, plasma defocusing at z = 32 m, and refocusing at z = 48 m. The data are for a slice on the leading edge (τ = –20 fs) of a 140-fs pulse with a wavelength of 0.8 μm, radius of 3.5 mm (e^{-1}), and energy of 10 mJ during filamentation in air [70]. Region *1* is a circle of 0.5 mm radius, region *2* is a ring with an inner radius of 0.5 mm and outer radius of 3.5 mm, and region *3* is a ring with an inner radius of 3.5 mm and outer radius of 8 mm.

Thus, a filament is a continuous sequence of regions of light focusing in temporal pulse slices where the collapsing growth of intensity due to Kerr nonlinearity is limited by defocusing in the laser-induced plasma, which is accompanied by the formation of ring structures in the intensity distribution in the pulse 'tail'. If there is a dynamic balance between Kerr focusing and plasma defocusing in the temporal slices of a propagating pulse, the light localisation region, where a plasma is generated and the intensity reaches saturation, propagates in the filament together with the pulse. Dynamic localisation of light in a filament whose length considerably exceeds the Rayleigh length is maintained by the energy reservoir located on the periphery of the propagating beam. The feasibility of 'plasmaless' filamentation with intensity growth limited by higher order nonlinearities, which was discussed by Béjot et al. [71], obtained no reliable confirmation [72].

Light whose power exceeds many times the critical power for self-focusing undergoes multiple filamentation, which nucleates as a consequence of modulation instability [20] on amplitude and phase inhomogeneities in the plane of a transverse section or on refractive index fluctuations in a randomly inhomogeneous medium. In this process, the array of filaments form a dynamic ensemble in which, in the course of propagation, initially nucleated filaments give way to 'daughter' and 'granddaughter' filaments, etc., which emerge at intensity maxima upon interference of the fields generated by the filaments of the preceding order [73, 74]. Optimal external focusing conditions may lead to the formation of a few merging filaments and a new structure, a superfilament, similar in properties to a usual single filament, which, however, has a higher intensity and free electron density [75, 76].

3.4. Frequency–angular spectrum

Filamentation is accompanied by frequency–angular broadening of the spectrum of the pulse, which results from optical field self-phase modulation in space and time [77–79]. The nonlinear phase shift $\varphi_{nl}(r, t, z)$ of the electric field

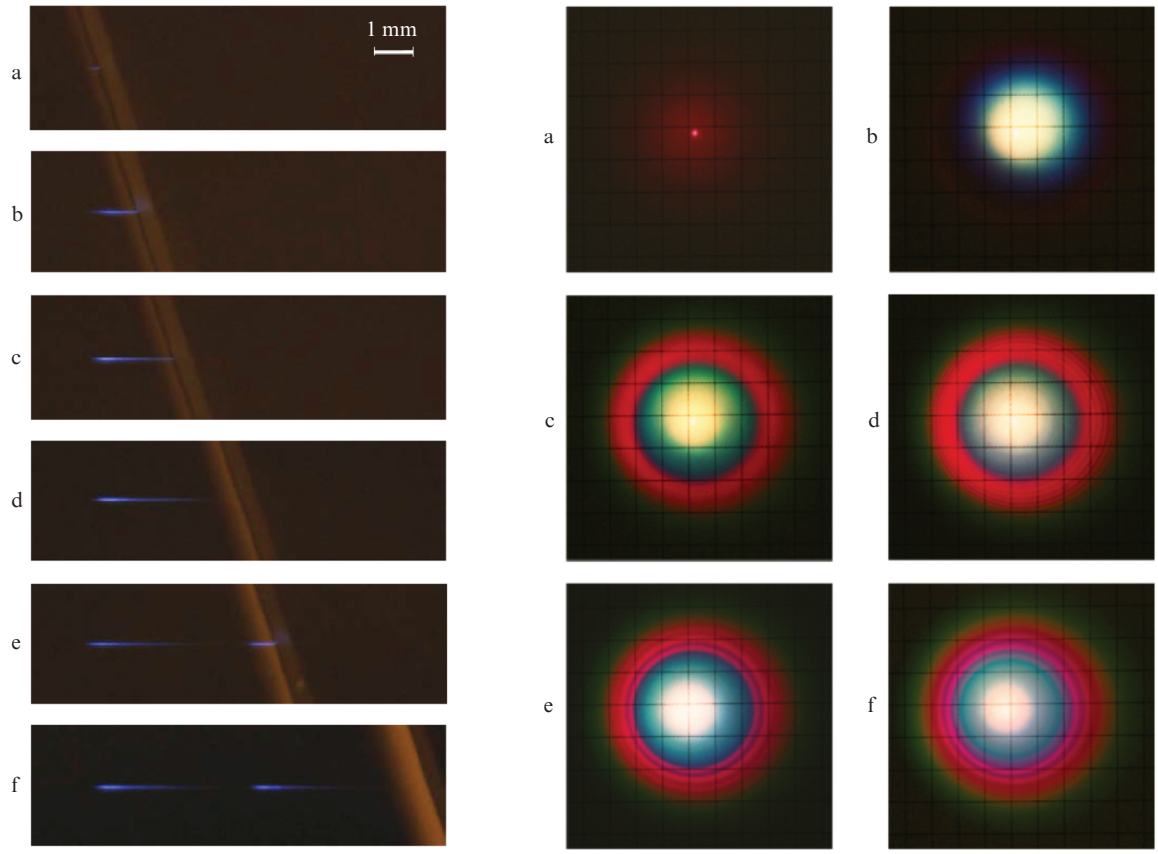

Figure 6. (Colour online) Variation of plasma channel luminescence (left) and supercontinuum light (right) with increasing propagation distance in fused silica for a 30-fs pulse at a wavelength of 0.8 μm (beam diameter, 100 μm; pulse energy, 2.4 μJ). (a) Symmetric broadening of the spectrum upon Kerr self-focusing, (b–d) anti-Stokes broadening of the spectrum upon filamentation, and (e, f) interference rings in the supercontinuum spectrum upon refocusing [82].

$$E(r,t,z) = E_0 \exp\{\mathrm{i}[\omega_0 t - k_0 z + \varphi_{\mathrm{nl}}(r,t,z)]\} \tag{3}$$

can be represented to second-order accuracy in a region of radius r^* and temporal slice t^* in the form

$$\varphi_{\mathrm{nl}}(r,t,z) \simeq \varphi_{\mathrm{nl}}(r^*, t^*, z) + \left.\frac{\partial \varphi_{\mathrm{nl}}}{\partial t}\right|_{r^*, t^*}(t - t^*) + \left.\frac{\partial \varphi_{\mathrm{nl}}}{\partial r}\right|_{r^*, t^*}(r - r^*). \tag{4}$$

The phase gradient with respect to time, $(\partial\varphi_{\mathrm{nl}}/\partial t)|_{r^*, t^*} = \Delta\omega(r^*, t^*)$, is a frequency increment, and the radial gradient $(\partial\varphi_{\mathrm{nl}}/\partial r)|_{r^*, t^*} = -\Delta k_{\mathrm{r}}(r^*, t^*)$ is an increment of the radial component of the wave vector. The nonlinear phase shift is determined by the refractive index increment in the nonlinear medium:

$$\varphi_{\mathrm{nl}}(r,t,z) = -k_0 \int_0^z \Delta n_{\mathrm{nl}}(r,t,z')\,\mathrm{d}z', \tag{5}$$

where $\Delta n_{\mathrm{nl}}(r, t, z) = \Delta n_{\mathrm{Kerr}}(r, t, z) + \Delta n_{\mathrm{pl}}(r, t, z)$.

On the leading pulse edge ($t < 0$), where there is no laser plasma, the Δn_{nl} increment is determined by Kerr nonlinearity, $\Delta n_{\mathrm{nl}}(r, t, z)|_{t<0} = n_2 I(r, t, z)/2n_0$, and the nonlinear phase is $\varphi_{\mathrm{nl}}(r, t, z)|_{t<0} \sim -I(r, t, z)$. Since the intensity $I(r, t, z)|_{t<0}$ increases with time, the emission spectrum on the leading edge acquires a Stokes shift $\Delta\omega|_{t<0} < 0$. The radial gradient of the phase is then positive ($\partial\varphi_{\mathrm{nl}}/\partial r|_{t<0} > 0$) and the Stokes signals converge to the axis: $\Delta k|_{t<0} < 0$. In the pulse tail ($t > 0$), $\Delta n_{\mathrm{nl}}(r, t, z)$ is dominated by plasma nonlinearity, and the refractive index increment $\Delta n_{\mathrm{nl}}(r, t, z)|_{t>0}$ decreases with increasing electron density $N_{\mathrm{e}}(r, t, z)$. Since the change in nonlinear phase is $\varphi_{\mathrm{nl}}(r, t, z)|_{t>0} \sim N_{\mathrm{e}}(r, t, z)$, which increases with time and decreases with increasing radial coordinate, the frequency and wave vector increments are $\Delta\omega|_{t>0} > 0$ and $\Delta k|_{t>0} > 0$, respectively. The temporal and radial gradients of the phase shift $\varphi_{\mathrm{nl}}(r, t, z)|_{t>0}$, proportional to plasma density $N_{\mathrm{e}}(r, t, z)$, considerably exceed the $N_{\mathrm{e}}(r, t, z)$ gradients, which are determined by Kerr nonlinearity on the leading pulse edge. Because of this, the anti-Stokes broadening and angular divergence of the spectrum far exceed the broadening and convergence of the Stokes signals on the leading edge. The intensity of spectral components of the supercontinuum decreases monotonically with increasing detuning from the carrier wavelength. At the same time, in the Stokes region the angular divergence of conical emission increases as the wavelength of spectral components decreases. Under refocusing conditions, there is interference of supercontinuum light from several generation sources in the filament, which are coherent in the case of self-phase modulation [80], and a ring structure emerges in the angular spectrum (Fig. 6) [81, 82] and a series of maxima appear in the frequency spectrum [83].

The transformation of a pulse during filamentation is significantly influenced by group velocity dispersion (GVD) [84, 85]. In the normal GVD regime ($\partial^2 k/\partial\omega^2 > 0$), under

Kerr nonlinearity conditions the pulse splits into two subpulses, which differ in group velocity and diverge with time during propagation (Fig. 7a). In the anomalous GVD regime ($\partial^2 k/\partial\omega^2 < 0$), the pulse compresses over time during filamentation in the bulk of a transparent medium, which opens up the possibility of formation of light bullets – wave packets compressed in both space and time (Fig. 7b).

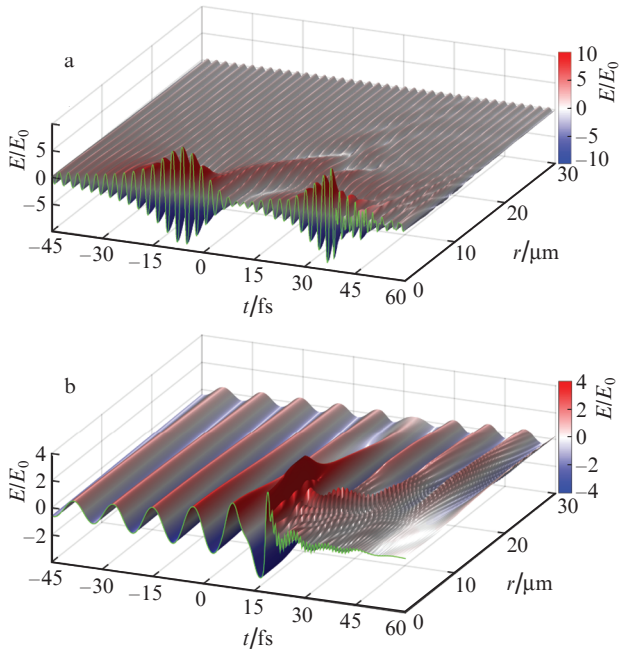

Figure 7. (Colour online) Electric field intensity in a wave packet for (a) filamentation at a normal GVD ($\lambda_0 = 0.8$ μm) and (b) LB formation at an anomalous GVD ($\lambda_0 = 3.1$ μm). The wave packet with $r_0 = 30$ μm and $2\tau_0 = 120$ fs propagates in LiF from right to left.

4. Light bullets

The term 'light bullets' was introduced by Silberberg [86]. Examining the quasi-optics equation for a pulse in a Kerr medium at an anomalous group velocity dispersion ($k_2 = \partial^2 k/\partial\omega^2 < 0$) in the paraxial approximation [11], he demonstrated the possibility of a spatiotemporal collapse of pulses. At an anomalous GVD, the quasi-optics equation in a moving frame in dimensionless coordinates for the complex amplitude $A(x, y, t, z)$ of a wave packet in a Kerr medium has the form

$$2\mathrm{i}\frac{\partial A}{\partial z} = \frac{\partial^2 A}{\partial x^2} + \frac{\partial^2 A}{\partial y^2} + \frac{L_{\mathrm{diffr}}}{L_{\mathrm{disp}}}\frac{\partial^2 A}{\partial t^2} + R\,|A|^2 A\,. \qquad (6)$$

Here, $L_{\mathrm{diffr}} = ka_0^2$ is the diffraction length of the wave packet; $L_{\mathrm{disp}} = \tau_0^2/|k_2|$ is its dispersion length; $2\tau_0$ is the 1/e pulse width; and R is the nonlinearity parameter, determining the nonlinear phase shift. For $L_{\mathrm{diffr}} \ll L_{\mathrm{disp}}$, the equation describes steady-state beam self-focusing. For $L_{\mathrm{diffr}} \gg L_{\mathrm{disp}}$, it describes pulse self-modulation in a Kerr medium. At $L_{\mathrm{diffr}} = L_{\mathrm{disp}}$, the spatial variables x and y and time t are equitable, which corresponds to simultaneous wave packet compression in space and time. This means that phase–amplitude conversion of the wave packet with a nonlinear phase shift occurs in time domain at an anomalous GVD in the same way as its conversion in the plane of a transverse section in the case of diffraction. The simultaneous wave packet compression in space and time leads to the formation of a light bullet: an extremely compressed wave packet a few optical field oscillations in width (Fig. 7b). In the case of wide-band-gap transparent dielectrics, such as fused silica and fluorides, the anomalous GVD region lies in the mid-IR, and advances in research on LBs depend on the advent of tunable sources based on femtosecond parametric oscillators.

4.1. Light bullet formation conditions

The effect of GVD on the dynamics of a pulse was demonstrated by Moll and Gaeta [87] in the case of light filamentation in a BK7 sample at wavelengths of 0.8 and 1.55 μm. The region where LBs exist in the space of variables that determine the wave packet energy and group velocity dispersion in a medium was found by Bergé and Skupin [88] by analysing integrals of motion of the equation for a slowly varying wave packet amplitude in a nonlinear Kerr medium. According to experimental data for sapphire and fused silica [89], an LB is formed at a sufficiently large parameter $|k_2|$, which determines anomalous GVD. At the same time, the concurrence of spatiotemporal wave packet compression depends on the relationship between the diffraction length L_{diffr} and dispersion length L_{disp}. The $L_{\mathrm{diffr}}/L_{\mathrm{disp}}$ ratio determines the threshold power P_{th} for LB formation, independent of the light wavelength and characteristics of the medium [90]. Increasing the $L_{\mathrm{diffr}}/L_{\mathrm{disp}}$ similarity parameter disturbs the concurrence of spatiotemporal wave packet compression and, as a consequence of its dispersion broadening, the ratio of the threshold power for LB formation to the critical power for steady-state self-focusing, $P_{\mathrm{th}}/P_{\mathrm{cr}}$, increases (Fig. 8). If the similarity parameter $L_{\mathrm{diffr}}/L_{\mathrm{disp}}$ approaches unity, increasing the pulse energy leads to the generation of a train of identical LBs as a result of time-domain light compression on the leading wave packet edge [91]. The spacing between LBs in the train is much smaller than that between the maxima in fluence after refocusing, which is due to the spatial light compression.

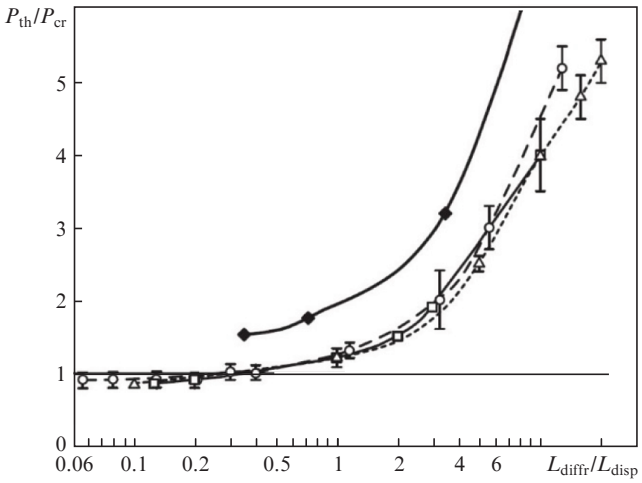

Figure 8. Ratio of the threshold power for LB formation to the critical power for steady-state self-focusing as a function of the $L_{\mathrm{diffr}}/L_{\mathrm{disp}}$ similarity parameter [experimental data for fused silica (♦) and numerical simulation data for fused silica (○), LiF (□), and CaF_2 (△) [90]].

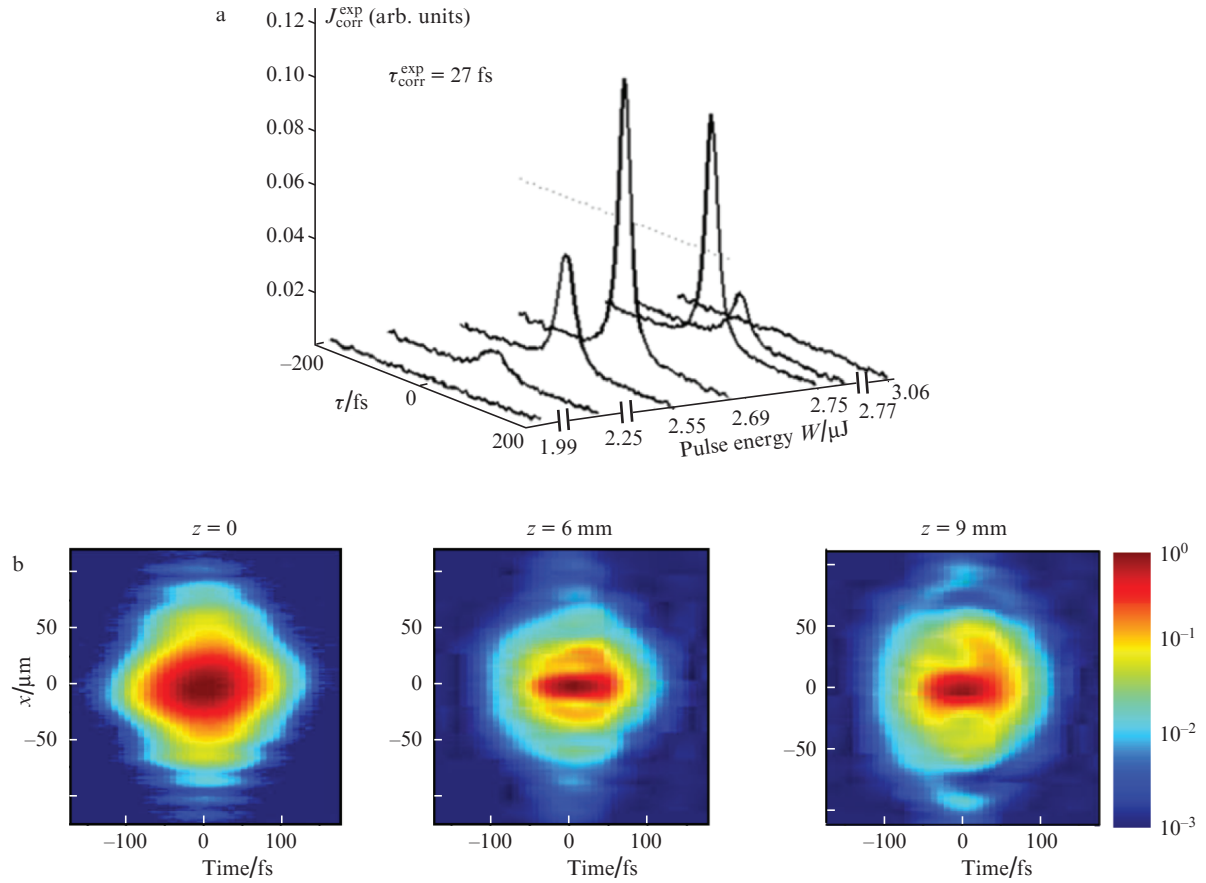

Figure 9. (Colour online) (a) Transformation of the measured autocorrelation trace in response to changes in the energy of a 50 fs (FWHM) pulse at a wavelength of 1.8 μm during filamentation in fused silica (sample length, 2 cm; selecting pinhole diameter, 50 μm [92]) and (b) spatiotemporal intensity distributions of an input wave packet and light bullet [62].

4.2. Light bullet parameters

The estimated LB duration is one to two optical oscillation periods. In particular, the LB duration in fused silica at a wavelength of 1.8 μm is 13.5 fs according to autocorrelation measurements, which corresponds to two optical field oscillations [92] (Fig. 9a), 20 fs according to spectral interference measurements [93], and 40–46 fs at an LB core diameter of 13 μm according to measurements on images of a spatially resolved cross-correlation function [62, 89, 94]. The LB duration in an YAG crystal at a wavelength of 3.1 μm is 32 fs according to FROG measurements, which corresponds to 2.9 optical periods [95]. The LB duration in KrS-5 and ZnSe in the far-IR spectral region at 9 μm is 45 fs as determined by autocorrelation measurements, which corresponds to 1.5 optical cycles [96].

The shape of LBs differs qualitatively from a Gaussian one, which has a significant effect on experimental data processing results. Besides, the estimated duration increases with an increase in the diameter of the pinhole separating the LB core with a high optical field intensity, whose cross-sectional size is much smaller than the diameter of the pinholes used. According to a number of reports [62, 89, 94], the diameter of the high-intensity LB core in fused silica and sapphire at a wavelength of 1.8 μm is 13–15 μm. Numerical estimates suggest that the measured LB duration at 1.8 μm in fused silica increases by a factor of 1.5 as the pinhole diameter increases from 50 to 100 μm [97, 98]. At a wavelength of 1.55 μm, the LB duration evaluated from a numerically obtained axial intensity profile is 5–10 fs [84, 88].

A light bullet is a few optical field oscillations whose amplitude varies strongly on an oscillation period timescale and on a wavelength scale in the plane of a transverse section (Fig. 7b), which makes its duration and radius difficult to determine. The concept of intensity for an LB of a few optical field oscillations, with a rapidly varying amplitude, is in conflict with all generally accepted definitions. An adequate characteristic of light localisation is the absolute square of the electric field intensity, $|E(r, t, z)|^2$. Analysis of the spatiotemporal electric field distribution allows ambiguity and contradiction in evaluation of LB parameters to be eliminated. The light bullet core S_{HF}, characterising optical field localisation, was defined previously [99] as the region of the wave packet in space and time where the electric field intensity meets the relation $|E(r, t, z)|^2 \geqslant e^{-1} \max_t |E(r, t, z)|^2$ (Fig. 10).

The temporal extent of the S_{HF} region on the beam axis is the local duration $2\tau_e(z)$, and its maximum cross-sectional size is the local LB core diameter $2r_e(z)$. Along with the local parameters, it is possible to introduce the effective parameters $2\tau_{eff}(z)$ and $2r_{eff}(z)$, in which the duration and radius are calculated with the weight $|E(r, t, z)|^2$, which takes into account the electric field redistribution in the wave packet. Both the local and effective durations and radii are a generalisation of the definition of the corresponding 1/e parameters of a Gaussian quasi-monochromatic wave packet to LBs. The

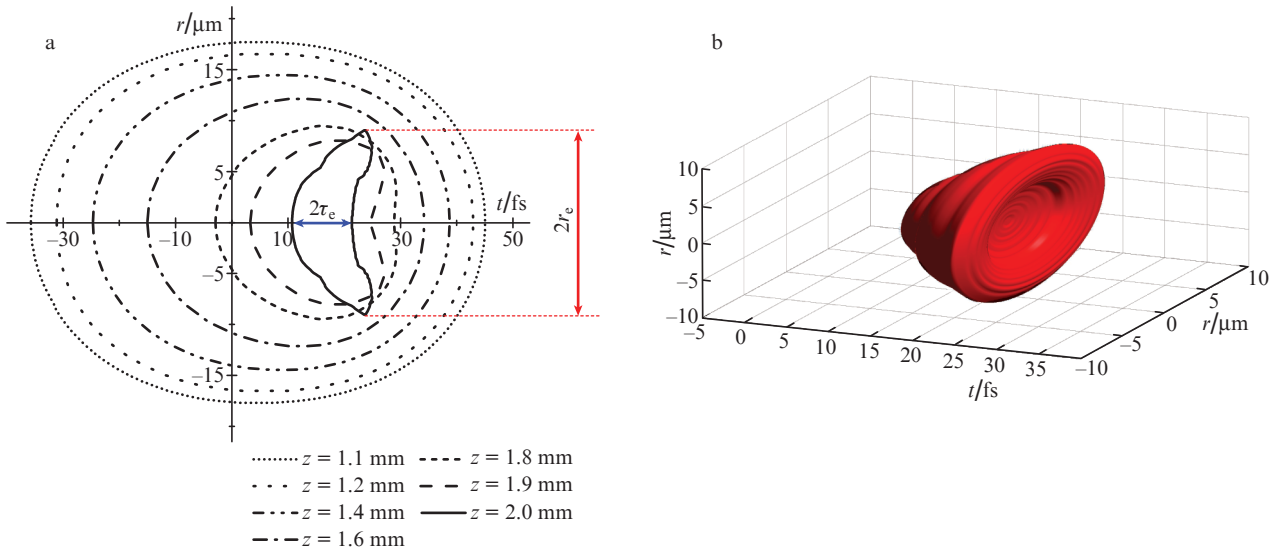

Figure 10. (Colour online) (a) Transformation of the high-field region during spatiotemporal wave packet compression in LiF [99] and (b) 3D image of this region in the resultant LB. A wave packet at a wavelength of $\lambda_0 = 3.1$ μm with a beam radius $r_0 = 30$ μm, pulse duration $\tau_0 = 120$ fs, and energy $W = 15.5$ μJ ($P = 1.4P_{cr}$) at an anomalous GVD propagates from right to left.

proposed approach is applicable for determination of LB parameters at any level of the absolute square of the field, e.g. 0.5 or $1/e^2$. The effective LB parameters are in fact the lower limit for experimental measurements.

4.3. Dynamics of a light bullet

During spatiotemporal wave packet compression, the S_{HF} region contracts monotonically, remaining similar to the original one, and wave packet parameters decrease monotonically to the point of the formation of an LB, with a qualitatively changed shape of its region (Fig. 10). The local duration of a kerne of an LB formed in LiF is about 2.5 optical oscillation periods, independent of wavelength λ_0, and its local diameter is $(2.5–6)\lambda_0$. During propagation of a light bullet, its core S_{HF} periodically contracts and expands in space and time (Fig. 11), which is accompanied by synchronous oscillations of all its parameters: radius, duration, peak electric field intensity, and energy $W_{HF}(z)$ localised in S_{HF} [100]. The oscillations result from changes in carrier–envelope phase (CEP) during propa-

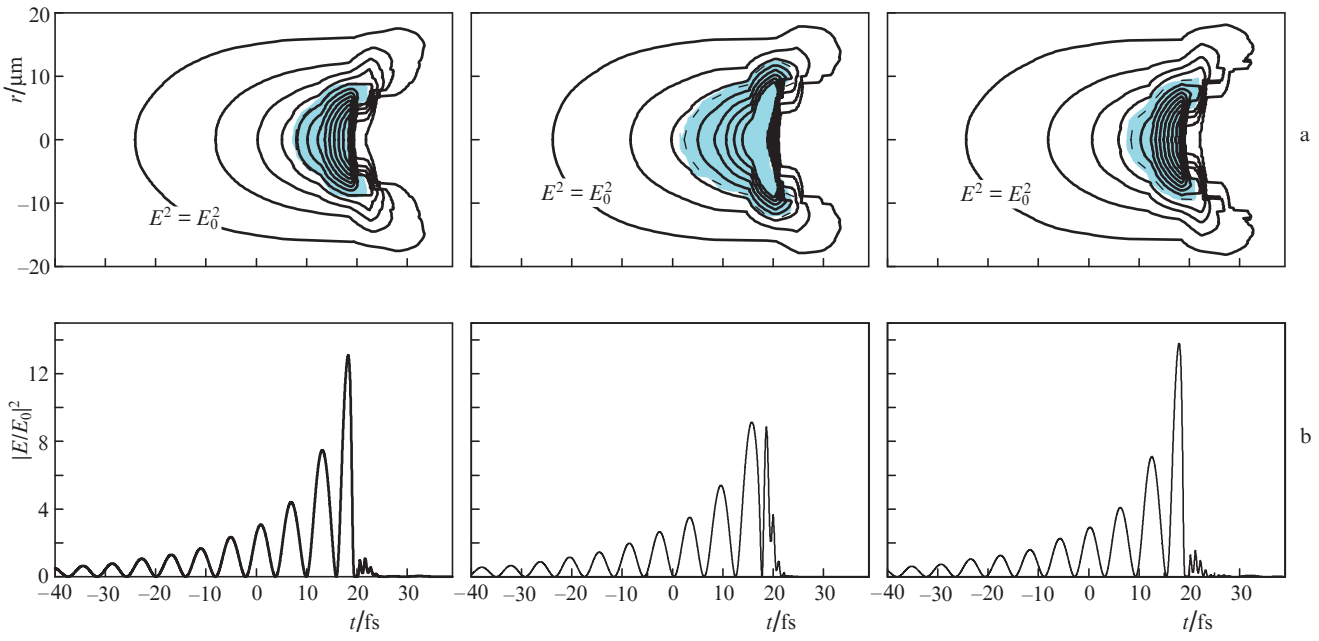

Figure 11. (Colour online) (a) Core oscillations during LB propagation in LiF: periodic compression and expansion of the core S_{HF} (the core is shown blue and its boundary is represented by a dashed line; the interval between the contour lines of the absolute square of the electric field intensity is E_0^2); (b) absolute square of the electric field intensity on the axis, $|E(r = 0, t)|^2$, when its maximum and minimum peak values at the nearest z are reached. The wavelength is 3.35 μm. The pulse propagates from right to left [100].

gation of an LB consisting of just a few optical field cycles. The oscillation period Δz decreases with increasing carrier wavelength λ_0 (Fig. 12), and it can be estimated using the following formula for a Gaussian pulse with a harmonic carrier [101, 102]:

$$\Delta z(\lambda_0) = \frac{\lambda_0 V_{gr}(\lambda_0)}{2n(\lambda_0)[V_{ph}(\lambda_0) - V_{gr}(\lambda_0)]}, \quad (7)$$

where $V_{ph}(\lambda_0)$ and $V_{gr}(\lambda_0)$ are the phase and group velocities in the dielectric at the carrier wavelength λ_0.

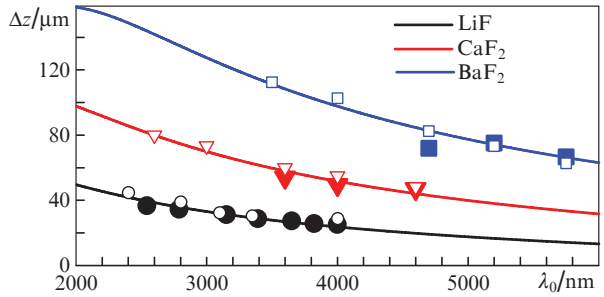

Figure 12. (Colour online) Effect of pulse wavelength λ_0 on the LB parameter oscillation period Δz determined numerically (open data points), analytically using relation (7) (solid lines), and experimentally (filled data points) for the concentration of colour centres in LiF and electron concentration in BaF_2 and CaF_2 [100].

In the case of circularly polarised light, there are no oscillations of LB parameters because the amplitude of the electric field vector always coincides with the maximum in the field envelope and remains unchanged during light propagation [103].

The 'breathing' of the LB as a result of CEP-induced oscillations of its parameters leads to periodic variations in the effectiveness of its nonlinear optical interaction over the path length in the medium, which were detected from the colour centre concentration in LiF [102, 104] and electron density in plasma channels induced in dielectrics during LB propagation (Fig. 13).

4.4. Spectrum of a light bullet

Filamentation of mid-IR light is accompanied by the generation of broadband supercontinuum, whose spectrum extends to the visible range and includes spectral components of the third, fifth, and subsequent odd harmonics of the fundamental frequency in the case of third-order nonlinearity and a continuous spectrum due to self-phase modulation [105–107]. Upon LB formation, anti-Stokes broadening completely spans carrier harmonics, whose spectral intensity oscillates because the phase matching condition is violated (Fig. 14). In the visible LB supercontinuum band, an isolated anti-Stokes wing, separated by a broad minimum from the carrier wavelength region, emerges. It is worth noting that, in the case of pulse filamentation in the normal GVD regime, the supercontinuum spectrum is narrower than the LB spectrum and remains monotonic throughout the wavelength range in question. An isolated anti-Stokes wing has been demonstrated experimentally for mid-IR light filamentation in a variety of materials [60, 61, 96, 98, 105, 108–115].

As the pulse wavelength and the band gap of the dielectric increase, the spectral band of the anti-Stokes wing decreases and shifts to shorter wavelengths [97, 116–120] (Fig. 15).

The frequency–angular spectrum of an LB is the result of the combined effect of the nonlinear process of broadband coherent supercontinuum generation upon the pulse self-phase modulation caused by Kerr and plasma nonlinearities and the linear process of supercontinuum interference in the anomalous GVD regime. From the constructive interference condition for the supercontinuum emitted by a propagating LB, the following dispersion equation for the shift $\Delta\lambda = \lambda_0 - \lambda_{SC}$ of the spectral maximum λ_{SC} of the anti-Stokes band of the supercontinuum can be obtained, which summarises all experimental data (Fig. 16) [106, 121]:

$$\Delta\lambda = [\lambda_0 n(\lambda_{SC}) - \lambda_{SC} n(\lambda_0)]\frac{V_{gr}}{c_0}, \quad (8)$$

where $n(\lambda)$ is the dispersion relation for the medium.

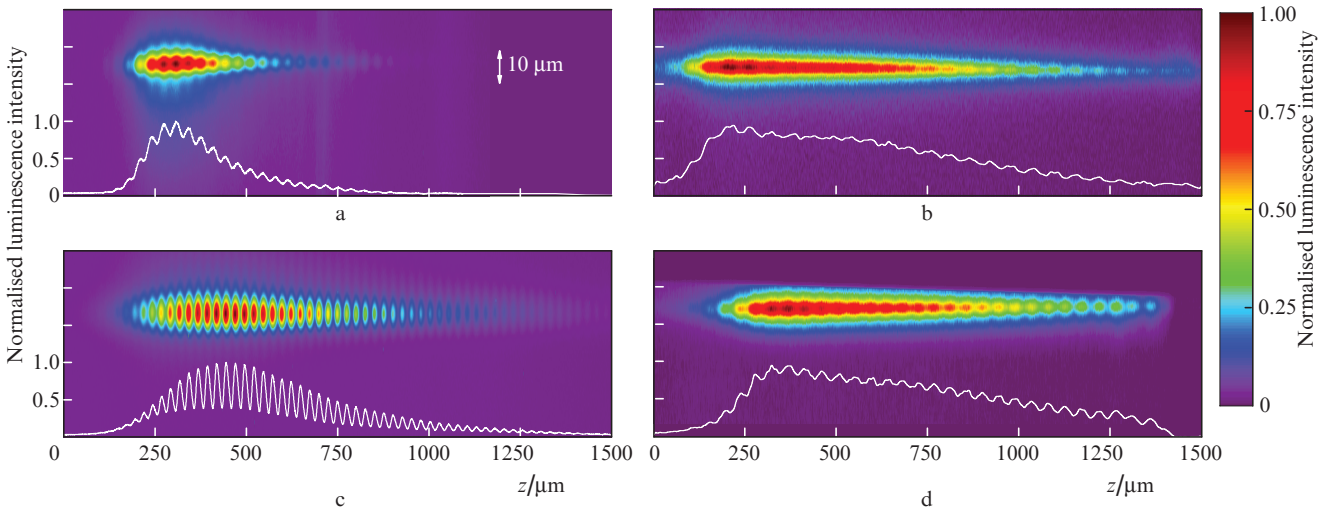

Figure 13. (Colour online) Spatial distributions of the luminescence intensity of colour centres induced in LiF by a light bullet at a wavelength of (a) 2.79 and (b) 4.0 μm and plasma luminescence in CaF_2 at a wavelength of (c) 3.6 and (d) 4.6 μm in the case of single-pulse exposure. The white lines represent the axial concentration profiles [100].

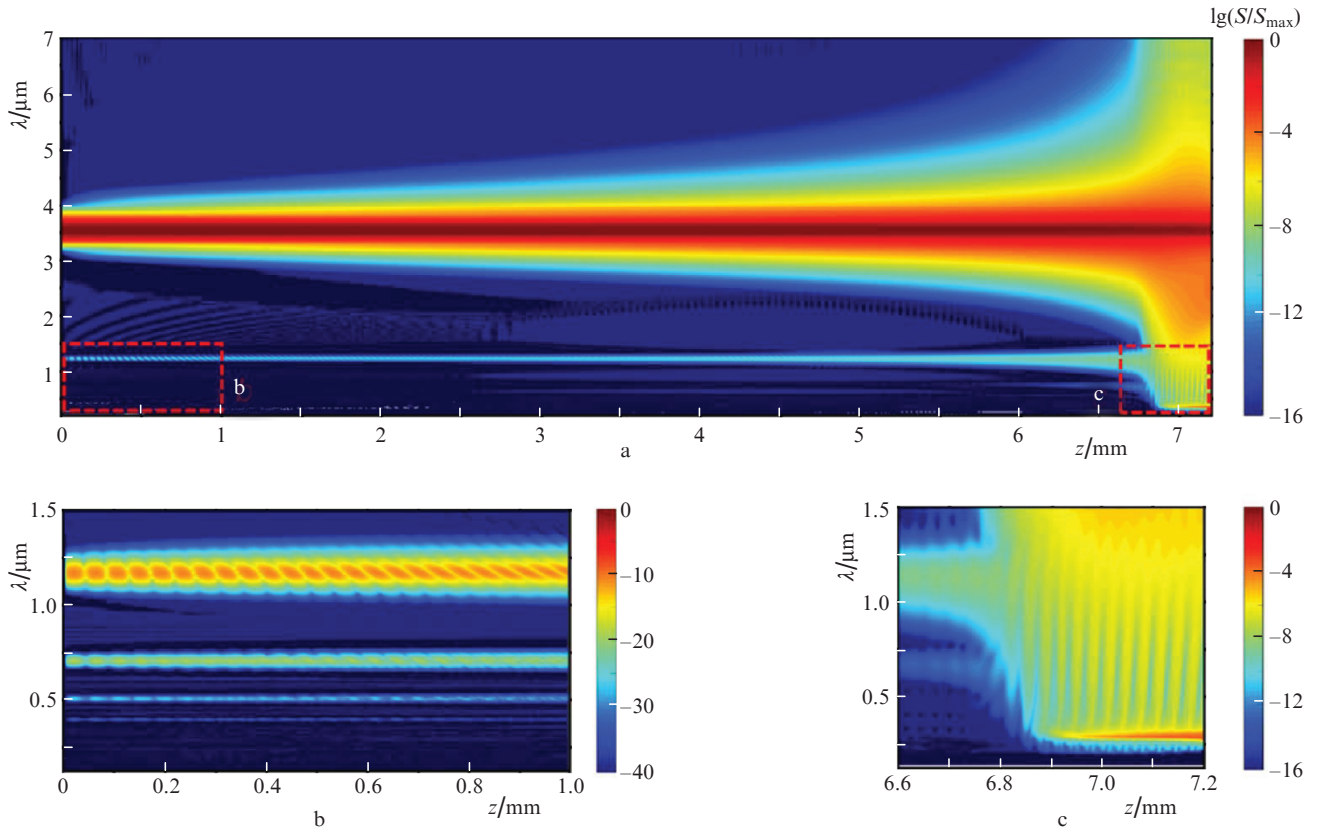

Figure 14. (Colour online) (a) Transformation of the spectrum of a 100-fs pulse with a wavelength of 3.5 μm and energy of 20 μJ as it propagates in LiF from the sample input until LB formation. (b) Spectrum of the third, fifth, and seventh harmonics generated at the beginning of pulse propagation; (c) broadband spectrum and anti-Stokes wing of the spectrum of the LB [106].

The short-wavelength cutoff of the anti-Stokes wing in the spectrum of mid-IR pulses in the anomalous GVD regime depends on their wavelength and the band gap of the dielectric and increases with increasing multiphoton ionisation order in the plasma generation process [106, 122]. The short-wavelength cutoff of the isolated anti-Stokes wing decreases

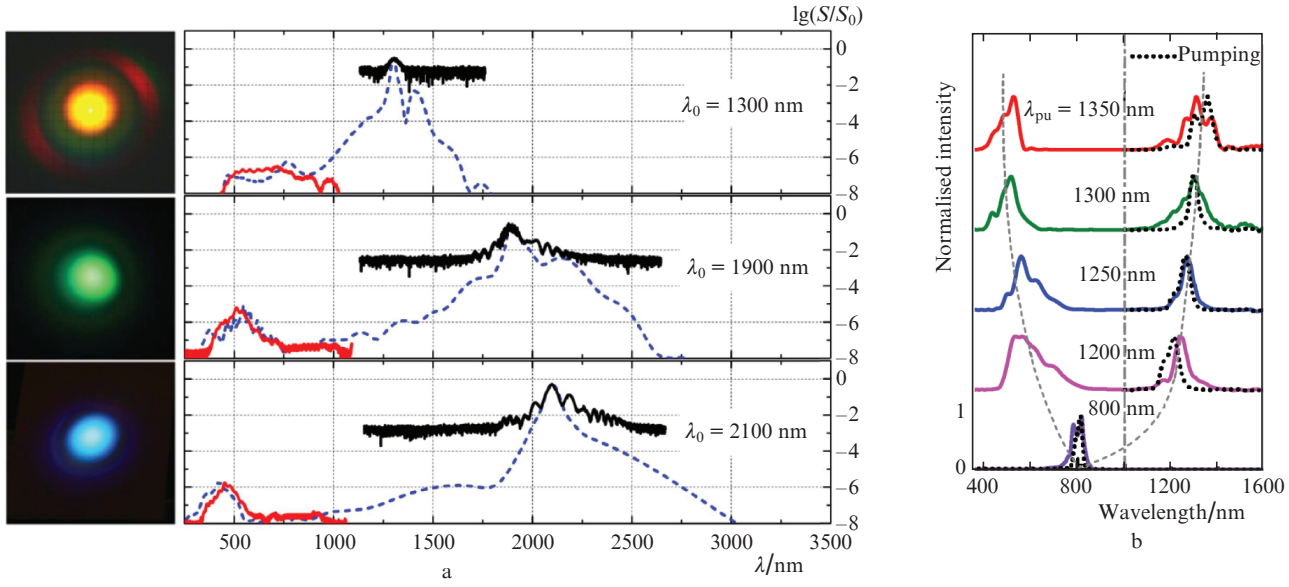

Figure 15. (Colour online) (a) Images of conical emission (left) and supercontinuum spectra (right) generated in fused silica by pulses at different wavelengths in the mid-IR spectral region (the solid lines represent the experimental data, and the dashed lines represent numerical simulation results; the pulse duration is τ_{FWHM} = 70 fs and the filament length in the wedge is 1 mm independent of wavelength; S_0 is the normalisation factor bringing the maxima of the simulated spectra in coincidence with those of the measured spectra [61, 106]). (b) Normalised spectra of a light bullet generated in water by pulses at wavelengths of 0.8, 1.2, 1.25, 1.3, and 1.35 μm, whose spectra are shown by dashed lines [118].

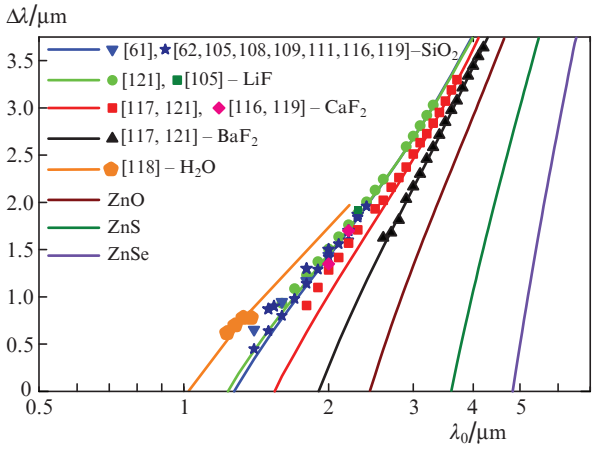

Figure 16. (Colour online) Shift $\Delta\lambda$ of the peak wavelength λ_{SC} of the anti-Stokes band of the supercontinuum against the carrier wavelength λ_0 of a laser pulse for filamentation in the anomalous GVD regime in various materials (the solid lines represent calculation results and the symbols represent experimentally measured $\Delta\lambda$) [108].

in a very short interval upon the collapsing growth of intensity in the emerging LB, which causes a sharp increase in self-phase modulation and, as a consequence, a precipitous anti-Stokes broadening of the spectrum. The shift of the short-wavelength cutoff to the anti-Stokes region is about 100 nm over 100 μm of pulse propagation in the medium upon LB formation [123, 124].

Numerical simulation in the axial symmetry approximation shows that, in vortex beams with a topological charge $m = 1$, a sequence of narrow annular LBs is formed and their radius and width decrease to 100 and 10 μm, respectively. The duration of the annular LBs is about 10 fs at a wavelength of $\lambda_0 = 1.8$ μm upon self-action in fused silica. Unlike in unimodal LBs formed in Gaussian beams, in annular LBs the collapsing growth of intensity upon self-focusing is limited not by the plasma, whose density is seven orders of magnitude lower than the density of neutrals, but by diffraction of annular arc elements, which is similar to diffraction of a 'slit' beam [125, 126].

4.5. Light bullets in the atmosphere

The possibility of LB formation in the atmosphere was first suggested by Shim et al. [127], who numerically examined pulse filamentation at a wavelength of 3.1 μm in humid air, whose dispersion was approximated using the HITRAN database and an algorithm proposed by Mathar [128]. Simulations were carried out at 10% air humidity, and the anomalous GVD parameter was evaluated at this humidity in a narrow spectral range from 3.0 to 3.2 μm: $k_2 = -0.53$ fs^2 cm^{-1}. At a wavelength of 3.1 μm, pulse duration of 150 fs, beam radius of 12 mm, peak power $P_{peak} = (2-4)P_{cr}$ (where $P_{cr} =$ 66 GW), and propagation distance of 450 m, spatiotemporal wave packet compression turned out to be relatively small because of the small width of the anomalous GVD region. At a broader anomalous GVD band with $k_2 = -1.25$ fs^2 cm^{-1}, wavelengths near 3.8 μm, a pulse duration of 120 fs, beam radius of 1 cm, pulse energy of 100 mJ, and propagation distance of 23 m, an LB of a few optical oscillations was formed, with an intensity of 10^{13} W cm^{-2} [98]. Numerical simulation results on light filamentation at a wavelength of 4 μm, pulse duration of 24 fs (FWHM), beam radius of 1.5 cm, and pulse energy of 177 mJ [129] predict the formation of an LB over a distance of 30 m in atmospheric air, with a high-intensity 5 × 5 mm core accounting for 14% to 18% of the pulse energy. The core of the LB then carries light with a peak power above 1 TW, which is maintained over a 30-m interval at a pulse energy of 177 mJ, and light with a power above 1.5 TW over a 50-m interval at a pulse energy of 315 mJ (Fig. 17). In a cuvette containing the $^{13}CO_2$ isotope, a 3.5-ps pulse with a wavelength of 10.3 μm and power of 7 TW would be expected to be compressed to 300 fs [130].

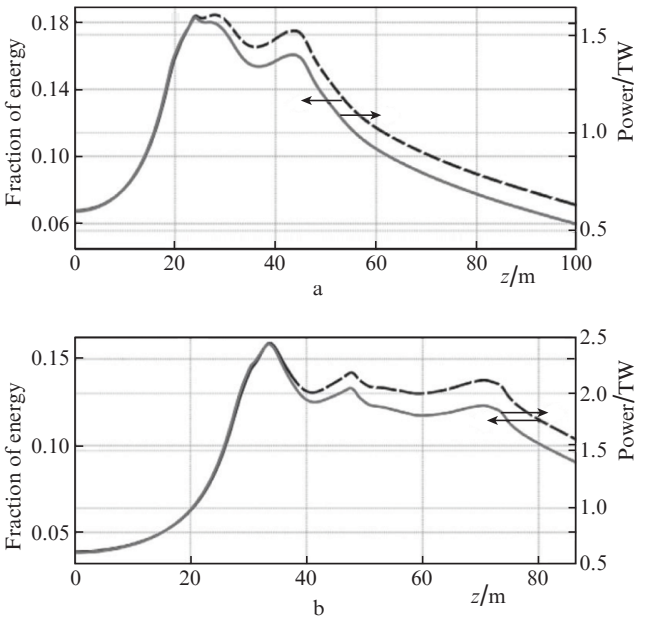

Figure 17. Fraction of energy (dashed line) and peak power (solid line) of a 5 × 5 mm core in a light bullet formed in air during propagation of 24-fs pulses with a wavelength of 4 μm (a) at an energy of 177 mJ and radius of 1.5 cm and (b) at an energy of 315 mJ and radius of 2 cm [129].

Spatiotemporal light compression in air was demonstrated experimentally by Mitrofanov et al. [131] for a propagating pulse with a wavelength of 3.9 μm, duration of 100 fs, and energy of 25 mJ. Phase modulation of a focused pulse reduces the LB duration to 28–32 fs [132].

4.6. Robustness of LBs

Light bullets are the result of self-organisation of a high-intensity optical field in a nonlinear medium at an anomalous group velocity dispersion. They are robust structures whose properties are determined by the nonlinear and dispersion properties of the medium and are independent of spatial or temporal characteristics of light. LBs can be formed in both spectrally limited light and phase-modulated light, which can be collimated or focused by a lens or axicon [98]. In solid dielectrics, the LB path length is about 500 μm, the estimated peak intensity is $5 \times (10^{13} - 10^{14})$ W cm^{-2}, the energy of the high-field LB core is 1–1.5 μJ, and the electron density in the laser-induced plasma channel is 10^{16} to 10^{20} cm^{-3} [84, 85, 95, 99, 133]. The LB path length, the bandwidth, and the maximum spectral intensity of the anti-Stokes wing of the supercontinuum are independent of the initial pulse energy [134]. Increasing the pulse energy leads to the

formation of a sequence of LBs identical in parameters [91]. Each LB in the sequence generates light in the anti-Stokes wing of equal energy (Fig. 18) [98, 135]. In vortex beams of femtosecond light, narrow annular light bullets are formed in which the intensity on their axis is zero because of the destructive interference of the optical field with phase dislocation.

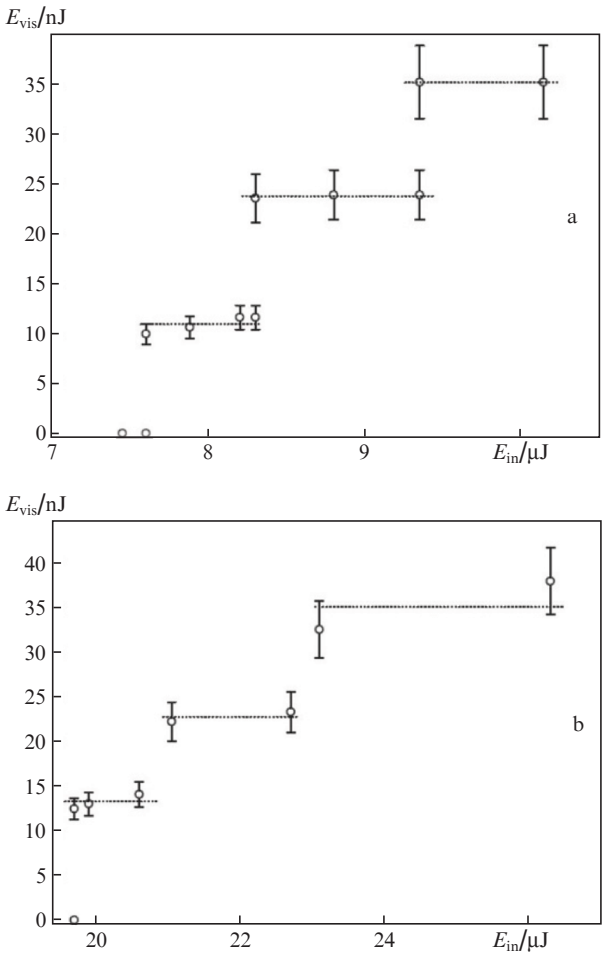

Figure 18. Variation in the energy of visible supercontinuum (E_{vis}) in the range $\lambda = 300-700$ nm upon the formation of subsequent LBs with increasing input pulse energy (E_{in}) at λ_0 = (a) 1.7 and (b) 1.9 μm [135].

A light bullet retains the capability of self-restoration in a nonlinear dispersive medium after both free diffraction in air over an interval no greater than 1000 μm and total internal reflection [136–139].

The study of light bullets, which are characterised by extreme optical field localisation and a broad spectrum, opens up fundamentally new possibilities for advances in nonlinear optical research methods with high spatial and temporal resolution, remote broadband probing methods, nonlinear fluorescence and emission spectroscopy of the environment, and long-haul transport of high-power energy.

Acknowledgements. This work was supported by the Russian Science Foundation (Grant No. 18-12-00422).

References

1. Kartashov Y.V., Malomed B.A., Torner L. *Rev. Mod. Phys*., **83**, 247 (2011).
2. Askar'yan G.A. *J. Exp. Theor. Phys.*, **15**, 943 (1962) [*Zh. Eksp. Teor. Fiz.*, **42**, 1360 (1962)].
3. Pilipetskii N.F., Rustamov A.R. *JETP Lett*., **2**, 88 (1965) [*Pis'ma Zh. Eksp. Teor. Fiz*., **2**, 55 (1965)].
4. Hercher M. *J. Opt. Soc. Am*., **54**, 563 (1964).
5. Boyd R.W., Lukishova S.G., Shen Y.R. *Self-focusing: Past and Present: Fundamentals and Prospects (Topics in Applied Physics)* (New York: Springer New York, 2009).
6. Basov N.G., Kryukov P.G., Senatskii Yu.V., Chekalin S.V. *J. Exp. Theor. Phys*., **30**, 641 (1970) [*Zh. Eksp. Teor. Fiz.*, **57**, 1175 (1970)].
7. Chiao R.Y., Garmire E., Townes C.H. *Phys. Rev. Lett*., **13**, 479 (1964).
8. Talanov V.I. *Izv. Vyssh. Uchebn. Zaved., Radiofiz*., **7**, 491 (1964).
9. Zakharov V.E., Sobolev V.V., Synakh V.S. *J. Exp. Theor. Phys*., **33**, 77 (1971) [*Zh. Eksp. Teor. Fiz*., **60**, 136 (1971)].
10. Akhmanov S.A., Sukhorukov A.P., Khokhlov R.V. *J. Exp. Theor. Phys*., **23**, 1025 (1966) [*Zh. Eksp. Teor. Fiz.*, **50**, 1537 (1966)].
11. Akhmanov S.A., Sukhorukov A.P., Khokhlov R.V. *Sov. Phys. Usp.*, **10**, 609 (1968) [*Usp. Fiz. Nauk*, **93**, 19 (1967)].
12. Marburger J.H. *Prog. Quantum Electron*., **4**, 35 (1975).
13. Fibich G., Gaeta A.L. *Opt. Lett*., **25**, 335 (2000).
14. Gol'dberg V.N., Talanov V.I., Erm R.E. *Izv. Vyssh. Uchebn. Zaved., Radiofiz*., **10**, 674 (1967).
15. Kandidov V.P., Fedorov V.Yu. *Quantum Electron*., **34**, 1163 (2004) [*Kvantovaya Elektron*., **34**, 1163 (2004)].
16. Dyshko A.L., Lugovoi V.N., Prokhorov A.M. *JETP Lett*., **6**, 655 (1967) [*Pis'ma Zh. Eksp. Teor. Fiz.*, **6**, 146 (1967)].
17. Dyshko A.L., Lugovoi V.N., Prokhorov A.M. *J. Exp. Theor. Phys.*, **34**, 1235 (1972) [*Zh. Eksp. Teor. Fiz*., **61**, 2305 (1972)].
18. DeMartini F., Townes C.H., Gustafson T.K., Kelley P.L. *Phys. Rev*., **164**, 312 (1967).
19. Akhmanov S.A., Vysloukh V.A., Chirkin A.S. *Optics of Femtosecond Laser Pulses* (New York: Am. Inst. of Physics, 1992; Moscow: Nauka, 1988).
20. Bespalov V.I., Talanov V.I. *JETP Lett*., **3**, 471 (1966) [*Pis'ma Zh. Eksp. Teor. Fiz*., **3**, 307 (1966)].
21. Basov N.G., Kertes I., Kryukov P.G., Senatskii Yu.V., Chekalin S.V. *J. Exp. Theor. Phys.,* **33**, 289 (1971) [*Zh. Eksp. Teor. Fiz*., **60**, 533 (1971)].
22. Kryukov P.G. *Quantum Electron*., **31**, 95 (2001) [*Kvantovaya Elektron*., **31**, 95 (2001)].
23. Kandidov V.P., Kosareva O.G., Brodeur A., Chin S.L. *Opt. Atmos. Okeana*, **10**, 1539 (1997).
24. Oleinikov P.A., Platonenko V.T. *Laser Phys*., **3**, 618 (1993).
25. Nibbering E.T.J., Grillon G., Franco M.A., Prade B.S., Mysyrowicz A. *J. Opt. Soc. Am. B*, **14**, 650 (1997).
26. Mlejnek M., Wright E.M., Moloney J.V. *Opt. Express*, **4**, 223 (1999).
27. Zheltikov A.M. *Opt. Lett*., **32**, 2052 (2007).
28. Braun A., Korn G., Liu X., Du D., Squier J., Mourou G. *Opt. Lett*., **20**, 73 (1995).
29. Nibbering E.T.J., Curley P.F., Grillon G., Prade B.S., Franco M.A., Salin F., Mysyrowicz A. *Opt. Lett*., **21**, 62 (1996).
30. Brodeur A., Chien C.Y., Ilkov F.A., Chin S.L., Kosareva O.G., Kandidov V.P. *Opt. Lett*., **22**, 304 (1997).
31. Chin S.L., Hosseini S.A., Liu W., Luo Q., Théberge F., Aközbek N., Becker A., Kandidov V.P., Kosareva O.G., Schroeder H. *Can. J. Phys*., **83**, 863 (2005).
32. Couairon A., Mysyrowicz A. *Phys. Rep*., **441**, 47 (2007).
33. Bergé L., Skupin S., Nuter R., Kasparian J., Wolf J.-P. *Rep. Prog. Phys*., **70**, 1633 (2007).
34. Kandidov V.P., Shlenov S.A., Kosareva O.G. *Quantum Electron*., **39**, 205 (2009) [*Kvantovaya Elektron*., **39**, 205 (2009)].
35. Chekalin S.V., Kandidov V.P. *Phys. Usp*., **56**, 123 (2013) [*Usp. Phys. Nauk*, **183**, 133 (2013)].
36. Yamada K., Watanabe W., Toma T., Itoh K., Nishii J. *Opt. Lett*., **26**, 19 (2001).
37. Abdollahpour D., Suntsov S., Papazoglou D.G., Tzortzakis S. *Opt. Express*, **19**, 16866 (2011).
38. Dergachev A.A., Ionin A.A., Kandidov V.P., Seleznev L.V., Sinitsyn D.V., Cunchugasheva E.S., Shlenov S.A. *Quantum Electron*., **43**, 29 (2013) [*Kvantovaya Elektron*., **43**, 29 (2013)].

39. Schillinger H., Sauerbrey R. *Appl. Phys. B: Lasers and Optics*, **68**, 753 (1999).
40. Tzortzakis S., Franco M.A., André Y.-B., Chiron A., Lamouroux B., Prade B.S., Mysyrowicz A. *Phys. Rev. E*, **60**, R3505 (1999).
41. Tzortzakis S., Prade B., Franco M., Mysyrowicz A. *Opt. Commun*., **181**, 123 (2000).
42. Lu X., Chen S.-Y., Ma J.-L., Hou L., Liao G.-Q., Wang J.-G., Han Y.-J., Liu X.-L., Teng H., Han H.-N., Li Y.-T., Chen L.-M., Wei Z.-Y., Zhang J. *Sci. Rep*., **5**, 15515 (2015).
43. Chen S., Liu X.-L., Lu X., Ma J., Wang J., Zhu B., Chen L., Li Y. *Opt. Express*, **25**, 32514 (2017).
44. Chen Y.-H., Varma S., Antonsen T.M., Milchberg H.M. *Phys. Rev. Lett*., **105**, 215005 (2010).
45. Bodrov S., Bukin V., Tsarev M., Murzanev A., Garnov S., Aleksandrov N., Stepanov A. *Opt. Express*, **19**, 6829 (2011).
46. Gopal A., Minardi S., Tatarakis M. *Opt. Lett*., **32**, 1238 (2007).
47. Minardi S., Gopal A., Tatarakis M., Couairon A., Tamošauskas G., Piskarskas R., Dubietis A., Trapani P.D. *Opt. Lett*., **33**, 86 (2008).
48. Yu Y., Jiang L., Cao Q., Shi X., Wang Q., Wang G., Lu Y. *Appl. Phys*. A, **122**, 205 (2016).
49. Fujimoto M., Aoshima S., Hosoda M., Tsuchiya Y. *Opt. Lett*., **24**, 850 (1999).
50. Fujimoto M., Aoshima S., Hosoda M., Tsuchiya Y. *Phys. Rev. A*, **64**, 033813 (2001).
51. Fujimoto M., Aoshima S., Tsuchiya Y. *Opt. Lett*., **27**, 309 (2002).
52. Majus D., Jukna V., Tamošauskas G., Valiulis G., Dubietis A. *Phys. Rev. A*, **81**, 043811 (2010).
53. Matijošius A., Trull J., Di Trapani P., Dubietis A., Piskarskas R., Varanavičius A., Piskarskas A. *Opt. Lett*., **29**, 1123 (2004).
54. Jarnac A., Tamosauskas G., Majus D., Houard A., Mysyrowicz A., Couairon A., Dubietis A. *Phys. Rev. A*, **89**, 033809 (2014).
55. Yu J., Mondelain D., Kasparian J., Salmon E., Geffroy S., Favre C., Boutou V., Wolf J.-P. *Appl. Opt*., **42**, 7117 (2003).
56. Kartashov D.V., Kirsanov A.V., Kiselev A.M., Stepanov A.N., Bochkarev N.N., Ponomarev Yu.N., Tikhomirov B.A. *Opt. Express*, **14**, 7552 (2006).
57. Bychkov A.S., Cherepetskaya E.B., Karabutov A.A., Makarov V.A. *Laser Phys. Lett*., **13**, 085401 (2016).
58. Martynovich E.F., Kuznetsov A.V., Kirpichnikov A.V., Pestryakov E.V., Bagayev S.N. *Quantum Electron*., **43**, 463 (2013) [*Kvantovaya Elektron*., **43**, 463 (2013)].
59. Chekalin S.V., Kompanets V.O. *Opt. Spektrosk*., **127**, 94 (2019).
60. Smetanina E.O., Kompanets V.O., Chekalin S.V., Kandidov V.P. *Quantum Electron*., **42**, 920 (2012) [*Kvantovaya Elektron*., **42**, 920 (2012)].
61. Smetanina E.O., Kompanets V.O., Chekalin S.V., Dormidonov A.E., Kandidov V.P. *Opt. Lett*., **38**, 16 (2013).
62. Gražulevičiūtė I., Šuminas R., Tamošauskas G., Couairon A., Dubietis A. *Opt. Lett*., **40**, 3719 (2015).
63. Brabec T., Krausz F. *Phys. Rev. Lett*., **78**, 3282 (1997).
64. Couairon A. *Eur. Phys. J. D*, **27**, 159 (2003).
65. Kandidov V.P., Smetanina E.O., Dormidonov A.E., Kompanets V.O., Chekalin S.V. *J. Exp. Theor. Phys.*, **113**, 422 (2011) [*Zh. Eksp. Teor. Fiz*., **140**, 484 (2011)].
66. Kolesik M., Moloney J.V., Mlejnek M. *Phys. Rev. Lett*., **89**, 283902 (2002).
67. Kandidov V.P., Fedorov V.Yu., Tverskoi O.V., Kosareva O.G., Chin S.L. *Quantum Electron*., **41**, 382 (2011) [*Kvantovaya Elektron*., **41**, 382 (2011)].
68. Smetanina E.O., Kadan V.M., Blonskyi I.V., Kandidov V.P. *Appl. Phys. B*, **116**, 755 (2014).
69. Dubietis A., Gaižauskas E., Tamošauskas G., Di Trapani P. *Phys. Rev. Lett*., **92**, 253903 (2004).
70. Kandidov V.P., Kosareva O.G., Koltun A.A. *Quantum Electron*., **33**, 69 (2003) [*Kvantovaya Elektron*., **33**, 69 (2003)].
71. Béjot P., Kasparian J., Henin S., Loriot V., Vieillard T., Hertz E., Faucher O., Lavorel B., Wolf J.-P. *Phys. Rev. Lett*., **104**, 103903 (2010).
72. Kosareva O., Daigle J.-F., Panov N., Wang T., Hosseini S., Yuan S., Roy G., Makarov V., Leang Chin S. *Opt. Lett*., **36**, 1035 (2011).
73. Hosseini S.A., Luo Q., Ferland B., Liu W., Chin S.L., Kosareva O.G., Panov N.A., Aközbek N., Kandidov V.P. *Phys. Rev. A*, **70**, 033802 (2004).
74. Dachraoui H., Oberer C., Michelswirth M., Heinzmann U. *Phys. Rev. A*, **82**, 043820 (2010).
75. Point G., Brelet Y., Houard A., Jukna V., Milián C., Carbonnel J., Liu Y., Couairon A., Mysyrowicz A. *Phys. Rev. Lett*., **112**, 223902 (2014).
76. Pushkarev D.V., Mitina E.V., Uryupina D.S., Volkov R.V., Panov V.A., Karabutov A.A., Kosareva O.G., Savel'ev A.B. *JETP Lett*., **106**, 561 (2017) [*Pis'ma Zh. Eksp. Teor. Fiz*., **106**, 545 (2017)].
77. Kandidov V.P., Kosareva O.G., Golubtsov I.S., Liu W., Becker A., Akozbek N., Bowden C.M., Chin S.L. *Appl. Phys. B: Lasers and Optics*, **77**, 149 (2003).
78. Dubietis A., Tamošauskas G., Šuminas R., Jukna V., Couairon A. *Lith. J. Phys*., **57**, 113 (2017).
79. Zheltikov A. *J. Opt. Soc. Am. B*, **36**, A168 (2019).
80. Chin S.L., Brodeur A., Petit S., Kosareva O.G., Kandidov V.P. *J. Nonlinear Opt. Phys. Mater*., **08**, 121 (1999).
81. Dormidonov A.E., Kandidov V.P. *Laser Phys*., **19**, 1993 (2009).
82. Dormidonov A.E., Kandidov V.P., Kompanets V.O., Chekalin S.V. *Quantum Electron*., **39**, 653 (2009) [*Kvantovaya Elektron*., **39**, 653 (2009)].
83. Zaloznaya E.D., Kompanets V.O., Chekalin S.V., Dormidonov A.E., Kandidov V.P. *Quantum Electron*., **50**, 366 (2020) [*Kvantovaya Elektron*., **50**, 366 (2020)].
84. Bergé L., Skupin S. *Phys. Rev. Lett*., **100**, 113902 (2008).
85. Smetanina E.O., Dormidonov A.E., Kandidov V.P. *Laser Phys*., **22**, 1189 (2012).
86. Silberberg Y. *Opt. Lett*., **15**, 1282 (1990).
87. Moll K.D., Gaeta A.L. *Opt. Lett*., **29**, 995 (2004).
88. Bergé L., Skupin S. *Phys. Rev. E*, **71**, 065601 (2005).
89. Gražulevičiūtė I., Garejev N., Majus D., Jukna V., Tamošauskas G., Dubietis A. *J. Opt*., **18**, 025502 (2016).
90. Zaloznaya E.D., Kompanets V.O., Dormidonov A.E., Chekalin S.V., Kandidov V.P. *Quantum Electron*., **48**, 366 (2018) [*Kvantovaya Elektron*., **48**, 366 (2018)].
91. Zaloznaya E.D., Dormidonov A.E., Kandidov V.P. *Opt. Atmos. Okeana*, **29**, 184 (2016).
92. Smetanina E.O., Kompanets V.O., Dormidonov A.E., Chekalin S.V., Kandidov V.P. *Laser Phys. Lett*., **10**, 105401 (2013).
93. Durand M., Lim K., Jukna V., McKee E., Baudelet M., Houard A., Richardson M., Mysyrowicz A., Couairon A. *Phys. Rev. A*, **87**, 043820 (2013).
94. Majus D., Tamošauskas G., Gražulevičiūtė I., Garejev N., Lotti A., Couairon A., Faccio D., Dubietis A. *Phys. Rev. Lett*., **112**, 193901 (2014).
95. Hemmer M., Baudisch M., Thai A., Couairon A., Biegert J. *Opt. Express*, **21**, 28095 (2013).
96. Qu S., Chaudhary Nagar G., Li W., Liu K., Zou X., Hon Luen S., Dempsey D., Hong K.-H., Jie Wang Q., Zhang Y., Shim B., Liang H. *Opt. Lett*., **45**, 2175 (2020).
97. Chekalin S.V., Kompanets V.O., Smetanina E.O., Kandidov V.P. *Quantum Electron*., **43**, 326 (2013) [*Kvantovaya Elektron*., **43**, 326 (2013)].
98. Chekalin S.V., Dokukina A.E., Dormidonov A.E., Kompanets V.O., Smetanina E.O., Kandidov V.P. *J. Phys. B*, **48**, 094008 (2015).
99. Zaloznaya E.D., Dormidonov A.E., Kompanets V.O., Chekalin S.V., Kandidov V.P. *JETP Lett*., **113**, 787 (2021) [*Pis'ma Zh. Eksp. Teor. Fiz*., **113**, 817 (2021)].
100. Zaloznaya E., Kompanets V., Savvin A., Dormidonov A., Chekalin S., Kandidov V. *Carrier-Envelope Phase of a Light Bullet.* arXiv:2201.04357 (2022).
101. Brabec T., Krausz F. *Rev. Mod. Phys*., **72**, 545 (2000).
102. Kuznetsov A.V., Kompanets V.O., Dormidonov A.E., Chekalin S.V., Shlenov S.A., Kandidov V.P. *Quantum Electron*., **46**, 379 (2016) [*Kvantovaya Elektron*., **46**, 379 (2016)].
103. Dormidonov A.E., Zaloznaya E.D., Kandidov V.P., Kompanets V.O., Chekalin S.V. *JETP Lett*., **115**, 11 (2022) [*Pis'ma Zh. Eksp. Teor. Fiz.*, **115**, 15 (2022)].
104. Chekalin S.V., Kompanets V.O., Kuznetsov A.V., Dormidonov A.E., Kandidov V.P. *Laser Phys. Lett*., **13**, 065401 (2016).
105. Garejev N., Tamošauskas G., Dubietis A. *J. Opt. Soc. Am. B*, **34**, 88 (2017).
106. Chekalin S.V., Dormidonov A.E., Kompanets V.O., Zaloznaya E.D., Kandidov V.P. *J. Opt. Soc. Am. B*, **36**, A43 (2019).

107. Šuminas R., Marcinkevičiūtė A., Tamošauskas G., Dubietis A. *J. Opt. Soc. Am. B*, **36**, A22 (2019).
108. Saliminia A., Chin S.L., Vallée R. *Opt. Express*, **13**, 5731 (2005).
109. Naudeau M.L., Law R.J., Luk T.S., Nelson T.R., Cameron S.M., Rudd J.V. *Opt. Express*, **14**, 6194 (2006).
110. Dharmadhikari A.K., Rajgara F.A., Mathur D. *Appl. Phys. B*, **82**, 575 (2006).
111. Durand M., Lim K., Jukna V., McKee E., Baudelet M., Houard A., Richardson M., Mysyrowicz A., Couairon A. *Phys. Rev. A*, **87**, 043820 (2013).
112. Cheng S., Chatterjee G., Tellkamp F., Ruehl A., Miller R.J.D. *Opt. Lett*., **43**, 4329 (2018).
113. Marcinkevičiūtė A., Tamošauskas G., Dubietis A. *Opt. Mater*., **78**, 339 (2018).
114. Marcinkevičiūtė A., Jukna V., Šuminas R., Garejev N., Tamošauskas G., Dubietis A. *Results Phys.*, **14**, 102396 (2019).
115. Šuminienė A., Jukna V., Šuminas R., Tamošauskas G., Dubietis A. *OSA Continuum*, **4**, 911 (2021).
116. Dharmadhikari J.A., Deshpande R.A., Nath A., Dota K., Mathur D., Dharmadhikari A.K. *Appl. Phys. B*, **117**, 471 (2014).
117. Dormidonov A.E., Kompanets V.O., Chekalin S.V., Kandidov V.P. *Opt. Express*, **23**, 29202 (2015).
118. Vasa P., Dharmadhikari J.A., Dharmadhikari A.K., Sharma R., Singh M., Mathur D. *Phys. Rev. A*, **89**, 043834 (2014).
119. Darginavičius J., Majus D., Jukna V., Garejev N., Valiulis G., Couairon A., Dubietis A. *Opt. Express*, **21**, 25210 (2013).
120. Jukna V., Galinis J., Tamosauskas G., Majus D., Dubietis A. *Appl. Phys. B*, **116**, 477 (2014).
121. Dormidonov A.E., Kompanets V.O., Chekalin S.V., Kandidov V.P. *JETP Lett*., **104**, 175 (2016) [*Pis'ma Zh. Eksp. Teor. Fiz*., **104**, 173 (2016)].
122. Kandidov V.P., Kompanets V.O., Chekalin S.V. *JETP Lett*., **108**, 287 (2018) [*Pis'ma Zh. Eksp. Teor. Fiz*., **108**, 307 (2018)].
123. Zaloznaya E., Kompanets V., Dormidonov A., Geints I., Chekalin S., Kandidov V. *Appl. Phys. B*, **127**, 42 (2021).
124. Tian Y., Gong C., Hu X., Liu X. *Phys. Rev. A*, **104**, 043506 (2021).
125. Vasilyev E.V., Shlenov S.A., Kandidov V.P. *Laser Phys. Lett*., **15**, 115402 (2018).
126. Vasilyev E.V., Kandidov V.P., Kompanets V.O., Chekalin S.V., Shlenov S.A. *Izv. Ross. Akad. Nauk, Ser. Fiz.*, **83**, 1602 (2019).
127. Shim B., Schrauth S.E., Gaeta A.L. *Opt. Express*, **19**, 9118 (2011).
128. Mathar R.J. *J. Opt. A: Pure Appl. Opt*., **9**, 470 (2007).
129. Panagiotopoulos P., Whalen P., Kolesik M., Moloney J.V. *Nat. Photonics*, **9**, 543 (2015).
130. Panagiotopoulos P., Hastings M.G., Kolesik M., Tochitsky S., Moloney J.V. *OSA Continuum*, **3**, 3040 (2020).
131. Mitrofanov A.V., Voronin A.A., Rozhko M.V., Sidorov-Biryukov D.A., Fedotov A.B., Pugžlys A., Shumakova V., Ališauskas S., Baltuška A., Zheltikov A.M. *Optica*, **4**, 1405 (2017).
132. Shumakova V., Ališauskas S., Malevich P., Voronin A.A., Mitrofanov A.V., Sidorov-Biryukov D.A., Zheltikov A.M., Kartashov D., Baltuška A., Pugžlys A. *Opt. Lett*., **44**, 2173 (2019).
133. Chekalin S.V., Kompanets V.O., Dormidonov A.E., Kandidov V.P. *Quantum Electron*., **48**, 372 (2018) [*Kvantovaya Elektron*., **48**, 372 (2018)].
134. Chekalin S.V., Kompanets V.O., Zaloznaya E.D., Kandidov V.P. *Quantum Electron*., **49**, 344 (2019) [*Kvantovaya Elektron*., **49**, 344 (2019)].
135. Chekalin S.V., Kompanets V.O., Dokukina A.E., Dormidonov A.E., Smetanina E.O., Kandidov V.P. *Quantum Electron*., **45**, 401 (2015) [*Kvantovaya Elektron*., **45**, 401 (2015)].
136. Gražulevičiūtė I., Tamošauskas G., Jukna V., Couairon A., Faccio D., Dubietis A. *Opt. Express*, **22**, 30613 (2014).
137. Chekalin S., Dormidonov A., Kandidov V., Kompanets V. *Opt. Lett*., **45**, 1511 (2020).
138. Chekalin S., Kompanets V., Dormidonov A., Kandidov V. *Laser Phys. Lett*., **17**, 085401 (2020).
139. Kompanets V., Dormidonov A., Chekalin S. *Opt. Lett*., **46**, 3187 (2021).